Accepted Manuscript

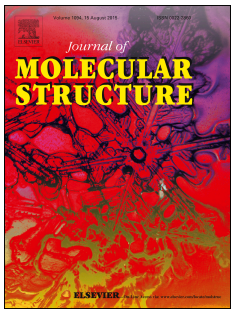

Crystal structure, thermal, luminescent and terahertz time domain spectroscopy of magnesium N-phthaloyl-β-alaninate: A combined experimental and theoretical study

Muhammad Nadeem, Moazzam H. Bhatti, Koray Sayin, Uzma Yunus, Mazhar Mehmood, Shoaib Mehboob, Ulrich Flörke

PII: S0022-2860(18)30631-8

DOI: 10.1016/j.molstruc.2018.05.063

Reference: MOLSTR 25236

To appear in: *Journal of Molecular Structure*

Received Date: 24 December 2017

Revised Date: 4 May 2018

Accepted Date: 19 May 2018

Please cite this article as: M. Nadeem, M.H. Bhatti, K. Sayin, U. Yunus, M. Mehmood, S. Mehboob, U. Flörke, Crystal structure, thermal, luminescent and terahertz time domain spectroscopy of magnesium N-phthaloyl-β-alaninate: A combined experimental and theoretical study, *Journal of Molecular Structure* (2018), doi: 10.1016/j.molstruc.2018.05.063.

Crystal structure, thermal, luminescent and terahertz time domain spectroscopy of magnesium N-phthaloyl-β-alaninate: A combined experimental and theoretical study

Muhammad Nadeem [a, c], Moazzam H. Bhatti [a]*, Koray SAYIN [b], Uzma Yunus [a], Mazhar Mehmood [c], Shoaib Mehboob [c], Ulrich Flörke [d]

[a] *Department of Chemistry, Allama Iqbal Open University, Islamabad, Pakistan*

[b] *Department of Chemistry, Institute of Science, Cumhuriyet University 58140 Sivas – Turkey*

[c] *National Center for Nanotechnology, Department of Metallurgy and Materials Engineering, Pakistan Institute of Engineering and Applied Sciences (PIEAS), Nilore 45650, Islamabad, Pakistan*

[d] *Anorganische und Analytische Chemie, Fakultät für Naturwissenschaften, Universität Paderborn, Warburgerstrasse 100, D-33098 Paderborn, Germany*

E-mail of corresponding Author:

* moazzamhussain_b@yahoo.com (M.H. Bhatti).

Abstract

A magnesium complex using N-phthaloyl-β-alanine (NPA) as ligand was synthesized and its crystal structure was characterized by single-crystal X-ray diffraction analysis. The Fourier transformation infrared spectroscopy (FTIR), thermogravimetry (TG) and differential thermal analysis (DTA), fluorescence spectroscopy and terahertz time-domain spectroscopy (THz-TDS) were performed for magnesium N-phthaloyl-β-alaninate (MgNPA). The coordination geometry around Mg (II) has found to be distorted octahedral and the coordination mode of NPA in MgNPA is monodentate i.e. $\eta^1\mu^1$. The significant enhancement was observed in the emission intensity of MgNPA complex as compared to the ligand NPA during solid state photoluminescence spectroscopy. The computational investigations of the complex were carried out at B3LYP/6-31+G(d,p) level in gas phase to support our experimental results. The small energy gap between frontier molecular orbitals (FMOs) manifested that MgNPA is a very reactive, chemically soft and optically active complex. The terahertz time domain spectroscopy of the complex and ligand was performed in order to characterize as well as to find out refractive index and absorption coefficient in 0.2-3.2 THz frequency range. Both the complex and ligand shows the characteristic absorption peaks in this frequency range. The decrease in refractive index is observed by the complexation of NPA with Mg.

Keywords: N-phthaloyl-ß-alanine, Single X-ray, Terahertz time-domain spectroscopy (THz TDS), Fluorescence spectroscopy

1 Introduction

The coordination compounds have attained considerable attention owing to their potential applications like catalysis, as optical and magnetic materials [1-4]. Magnesium ion being most abundant in living things plays essential role in many biological processes [5]. The polarizing power of magnesium (II) is very dominant in s-block metals, therefore the coordination bond between magnesium (II) and oxygen is very strong providing some hybrid magnesium framework [6-9]. The complex solid structure architecture mainly depends upon the choice of organic ligand. ß-alanine has appeared to build up the concentration of carnosine in muscles, diminish weariness in athletes and enhance the efficiency of muscles [10]. The phthalimide group helps to provide supramolecular host design and also act as a protecting group for amino acids. Its fluorescence properties are highly environment sensitive [11]. N-phthaloyl-β-alanine contains highly conjugated phthalimide aromatic cyclic moiety. Nonlinear optical properties have been enhanced due to the presence phthalimide group in previously reported CaNPG complex [12]. For the support of experimental work quantum chemical calculations are significant research area for researchers [13-17].

In recent years, terahertz spectroscopy has attracted the attention of researchers for the study of vibrational modes in far infrared frequency range. It is used for the nondestructive testing [18], identification of drugs [19], and determination of dielectric properties of materials [20-24]. It is also used for the characterization of different biological molecules such as amino acids [25], aromatic carboxylic acids [26], proteins, DNA, bovine serum albumin and collagen [27], etc. Different organometallic complexes show the signature in THz frequency range [28-30]. These signatures can be used for the identification of the complex.

In this work we have reported the synthesis of new single crystal magnesium N-phthaloyl-β-alaninate (MGNPA) complex. This compound was characterized by Single-crystal X-ray diffraction analysis, FTIR, TG-DTA, UV-visible spectroscopy, NMR and THz TDS. Optimized compound structure, geometric parameters, vibration frequencies, contour diagram of frontier molecular orbitals (FMOs), molecular electrostatic potential (MEP) maps, MEP contours, NMR spectrum are investigated at B3LYP/6-31+G(d,p) level. The solid state photoluminescence of complex and ligand was performed in order to find out the optical properties of the complex.

2 Experimental

2.1 Synthesis of N-phthaloyl β-alanine

N-phthaloyl β-alanine was prepared by the reported methods [31]. In a Pyrex test tube, an equimolar amount of beta alanine and phthalic anhydride were fused using previously heated oil bath at 180-185^{o}C for fifteen minutes. After this, the test tube was carefully removed and cooled until the liquid mass was solidified. It was then inverted and the excess phthalic anhydride sublimed on the walls was scrapped out. The crude product was recrystallized in ethanol solvent.

2.2 Synthesis of MgNPA

An aqueous solution of sodium hydroxide (9.1mmol in 50ml) was added dropwise to a well-stirred solution of N-phthaloyl-β-alanine (9.1mmol) in ethanol (40 ml) at room temperature. The solution was stirred for next 2 h and then 4.5mmol of magnesium acetate [$Mg(CH_3COO)_2$] were added. The solution was heated to 80°C and stirred at this temperature for 2 h. The hot solution was filtered and set aside for crystallization. After four weeks, ~2g (41% yield) of colorless single crystals were obtained. The synthesis scheme, a) for ligand, and b) for complex is given below.

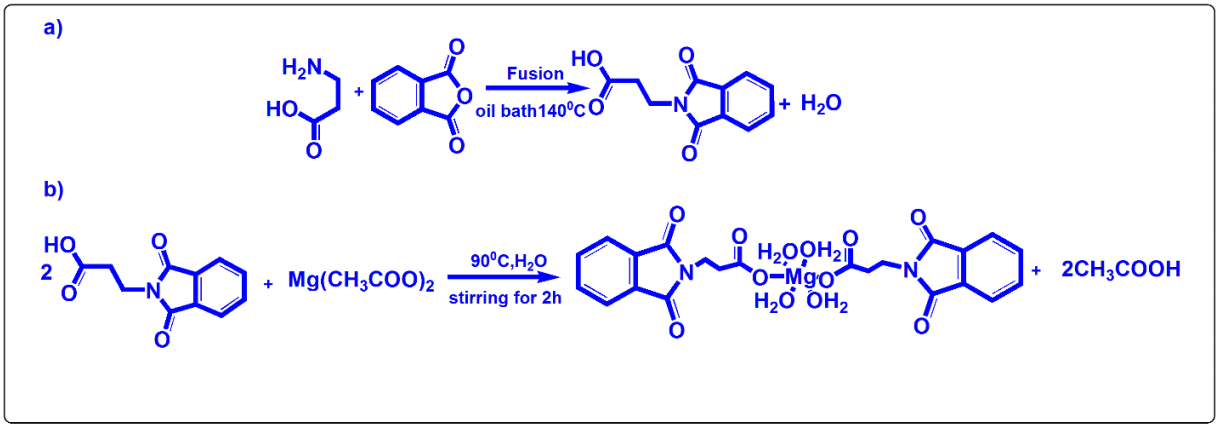

Scheme 1. (a) Synthesis of NPA and (b) MgNPA.

2.3 Computational Method

GaussView 5.0.9 [32] and Gaussian 09 AS64L-G09RevD.01 [33-37] package programs were used to do quantum chemical calculations. The graphs and figures were prepared by using different softwares as ChemBioDraw Ultra Version (13.0.0.3015), Gabedit, Chemissian and Chemcraft [38, 39]. B3LYP which is one of the hybrid density functional theory functions was selected as method with basis set, 6-31+G(d,p) [40, 41] for MgNPA. No imaginary frequency was obtained from the calculations.

2.4 Crystal structure determination

The intensity data for all compounds were recorded using a Bruker SMART CCD area-detector diffractometer with graphite monochromated Mo K_α radiation (λ = 0.71073 Å) at T = 130(2) K. Semi-empirical absorption correction applied from equivalents i.e. structure solutions by direct methods [42], full-matrix least squares refinements [42] based on F^2. All but H-atoms were refined an-isotropically, hydrogen atoms were clearly located from difference Fourier maps, refined at idealized positions riding on the parent atoms with isotropic displacement parameters U_{iso}(H) = 1.2U_{eq}(C/O) and C-H 0.95-0.98 Å.

2.5 Measurements

Infrared spectra were recorded for the free ligand and title complex on Nicolet iS 10 FTIR Spectrophotometer (4000-400 cm^{-1}) in KBr discs. Melting points were determined via Gallen Kamp electro thermal apparatus, Cat No.MPD350, sanyo, UK. UV-visible spectra of ligand solution and MgNPA solution in deionized water were recorded on UV-1800 Shimadzu using UV probe version 2.32 control software for Shimadzu UV-Vis(-NIR) spectrophotometers. The ^{1}H and ^{13}C nuclear magnetic resonance spectrum were recorded at room temperature in DMSO-d6 on a Bruker Avance Digital 300 MHz and 75 MHz spectrometer (Switzerland), respectively. Chemical shifts are given in ppm and coupling constant (*J*) values are given in Hz. Fluorescent emission spectra were recorded on F-7000 FL spectrophotometer 2133-007. Thermal decomposition patterns (TG and DTA) of the title compound was carried out under nitrogen atmosphere up to 800°C utilizing a heating rate of 10°C/min on a DTG-60H simultaneous DTA-TG Analyzer.

2.6 THz-Time Domain Spectroscopy

The THz measurements were performed using Femto Fiber Pro laser system from TOPTICA Photonics. The 100 fs laser pulses centered at 780 nm with average power of ~45mWweregenerated. Beam splitter was used to divide the laser beam into two parts. The THz pulses are generated and detected by focusing the laser power of ~30 mW and ~15 mW on photoconductive THz emitter and detector, respectively. All the measurements were performed in transmission mode. In order to reduce the effect of humidity, the measurement chamber was purged with N_2 gas.

The ground powder of MgNPA and NPA was placed in a cell with HDPE windows. HDPE windows are used because of low absorption of THz radiations in HDPE. The time domain

reference signal was recorded by passing THz radiations through the empty cell and the time domain sample signal was recorded by passing THz radiations through the cell filled with the powder. These time domain signals were fourier transformed to get complex frequency domain signals which were then used to calculate the refractive index and absorption coefficient of MgNPA and NPA. The detail of calculations can be found elsewhere [21].

3 Results and Discussions

3.1 Specific structural details

Single-crystal X-ray diffraction analysis reveals the formation of the magnesium complex [C_{44} H_{42} N_4 O_{20}Mg]. It was found MgNPA crystallized in monoclinic system with C2/c space group. The unit cell has dimensions a = 20.8884(17) Å, b = 19.8335(17) Å, c = 13.4979(11) Å, α= 90°, β = 129.319(2) °, γ = 90° with volume i.e. V= 4326.2(6) $Å^3$ and Z=4. The most relevant crystal data and structure refinement details are given in Table 1. Each magnesium atom is coordinated by six oxygen atoms i.e. two carboxylate oxygen atoms [O(4), O(4A)] in a monodentate manner ($\eta^1\mu^1$) and four with labeled oxygen atoms [O(9),O(9A),O(10), O(10A)] of water molecules. Out of four ligand molecules, the carbonyl groups of two n-phthaloyl ß-alanine molecules remained uncoordinated. The selected bond angles (deg) and bond lengths suggest the formation of distorted octahedral geometry around magnesium. The schematic of optimized and experimental structure with atomic labeling is shown in Fig. 1. The calculated thermo-dynamic parameters including total energy, enthalpy and Gibbs free energy of the complex are -2065.028007, -2065.027063 and -2065.143392 a.u., respectively. The selected experimental and calculated geometric parameters of magnesium complex are given in Table 2.

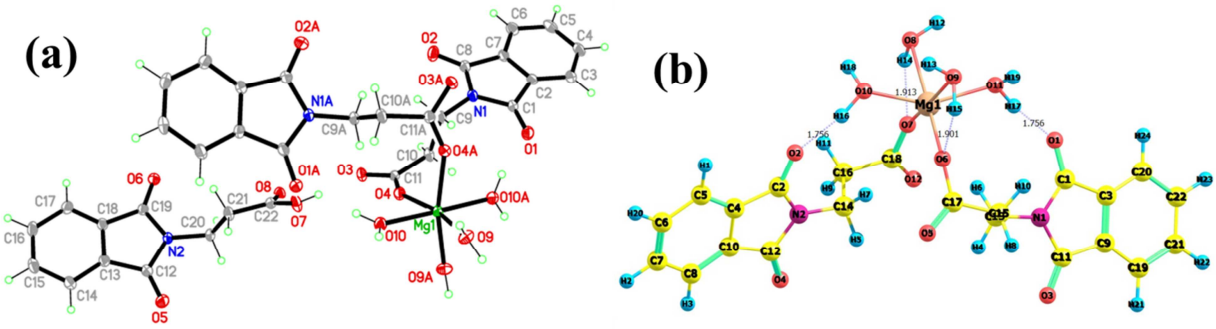

Fig. 1. (a) View of single X ray crystal Structure for MgNPA, anisotropic displacement ellipsoids are drawn at the 50% probability level (color codes: Mg, dark green; C, grey; O, red; N, blue; H, light green), symmetry transformations used to generate equivalent atoms for 2a: #1 -x,y,-z+1/2. (b) optimized structure of MgNPA at B3LYP/6-31+G(d,p) level.

Table 1. Crystal data and structure refinement details for MgNPA.

Parameters	MgNPA
Empirical formula	C_{44} H_{42} Mg N_4 O_{20}
Formula weight	971.13
T (K)	130(2) K
Wavelength (Å)	0.71073
Crystal system	Monoclinic
Space group	C2/c
a (Å)	20.8884(17)
b (Å)	19.8335(17)
c (Å)	13.4979(11)
α (°)	90
β (°)	129.319(2)
γ (°)	90
Volume (Å^3)	4326.2(6)
Z	4
D calc (Mg/m^3)	1.491
Absorption coefficient(mm^{-1})	0.132
F(000)	2024
Crystal size (mm^3)	0.38 x 0.21 x 0.18
θ(°) range	1.63 to 27.88
Reflections collected	20410
Independent reflections	5159
R(int)	0.0339
Completeness to θ = 27.88°	99.90%
Max. and min. transmission	0.9767 and 0.9516

Table 2. Experimental and theoretical bond lengths (Å) and bond angles (°) for MgNPA.

Assignments	Experimental	Calculated
Bond Lengths (Å)		
Mg1-O6 O4A	2.0489	1.9760
Mg1-O7 O4	2.0489	1.9763
Mg1-O8 O9A	2.0699	2.2364
Mg1-O9 O9	2.0699	2.2364
Mg1-O10 O10A	2.0561	2.1377
Mg1-O11 O10	2.0560	2.1368
Bond Angles (deg.)		
O6-Mg1-O7	93.72	107.37
O6-Mg1-O8	167.07	175.92
O6-Mg1-O9	90.36	76.22
O6-Mg1-O10	83.13	97.01
O6-Mg1-O11	96.21	99.08
O7-Mg1-O8	90.36	76.17
O7-Mg1-O9	167.07	175.97
O7-Mg1-O10	96.21	98.98
O7-Mg1-O11	83.13	97.18
O8-Mg1-O9	88.34	100.32
O8-Mg1-O10	84.23	80.28
O8-Mg1-O11	96.46	82.31
O9-Mg1-O10	96.46	82.24
O9-Mg1-O11	84.23	80.27
O10-Mg1-O11	179.04	152.61
Hydrogen Bond Lengths (Å)		
O8-H···O7	-	1.9127
O9-H···O6	-	1.9138
O10-H···O2	-	1.7565
O11-H···O1	-	1.7558

The four intramolecular hydrogen bonds present in the complex discussed in the Table 2 and graphically presented in Fig. 1 (b). The experimental and calculated geometric parameters were compared through distribution graph as shown in the Fig. 2. It was found that there is a good agreement between experimental and calculated structures.

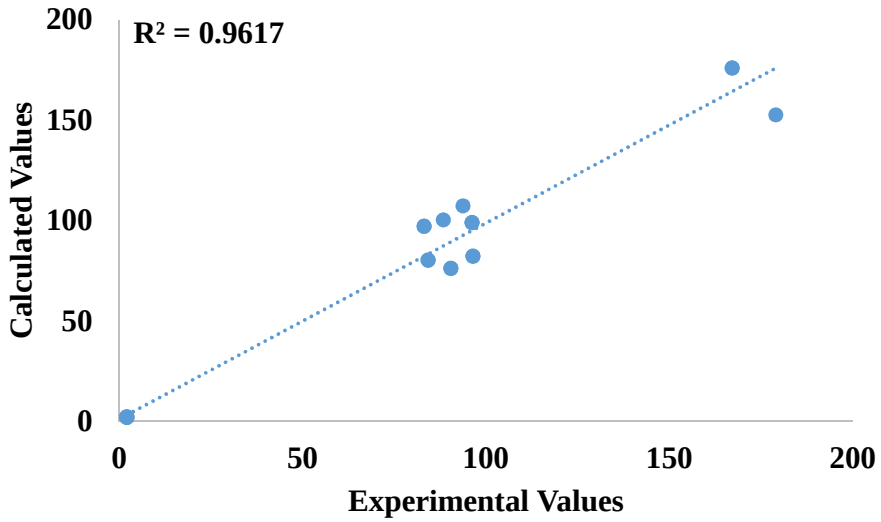

Fig. 2. Distribution graph between experimental and calculated geometric parameters.

3.2. FTIR spectroscopy

The FT-IR spectra for MgNPA and NPA along with theoretical IR spectrum of MgNPA are presented in Fig. 3. The modes assigned to the calculated and experimental vibrational frequencies are given in Table S1. The medium broad absorption in the experimental spectrum of MgNPA at 3448 cm^{-1} and 3397 cm^{-1} proved the presence of coordinated water molecule [43, 44]. The corresponding theoretical symmetric and asymmetric H_2O stretching vibrations are present at 3576 cm^{-1} and 3462 cm^{-1} respectively. The characteristic stretching vibrations of cyclic carbonyl related to the Phthalimide group appeared at 1763 and 1706 cm^{-1} in experimental spectrum, while in calculated spectrum these vibrations were found at 1740 and 1703 cm^{-1}. The asymmetric (ma) and symmetric (ms), due to the carboxylate group appeared at 1456 and 1232 cm^{-1} in experimental spectrum respectively. The phthalimide C-C ring stretching vibrations were observed experimentally and theoretically at 1363 cm^{-1} and 1352 cm^{-1}, respectively. In the low frequency region, the absorption bands at 519 and 460 cm^{-1} in experimental IR and at 528, 478, 466 cm^{-1} in theoretical IR are related to Mg-O vibrations.

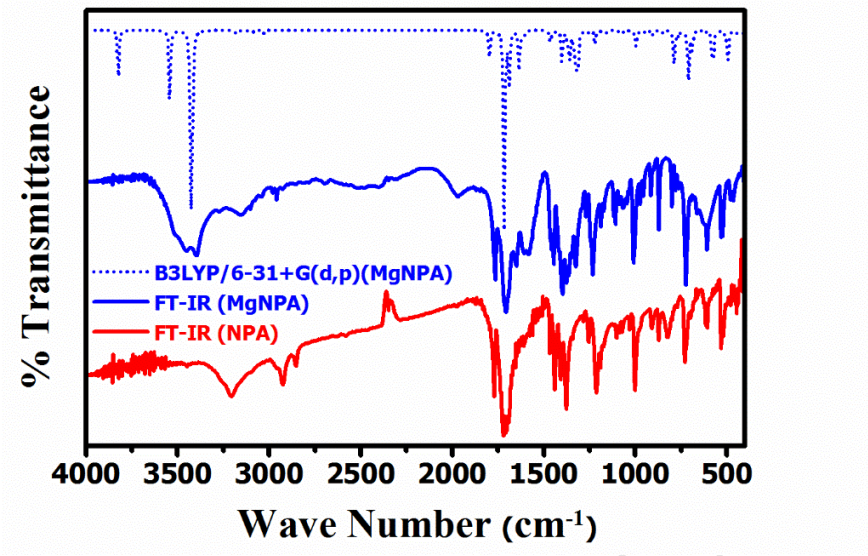

Fig. 3. FTIR spectrum of NPA and MgNPA in KBr disc alongwith calculated IR spectrum at B3LYP/6-31+G(d,p) level in vacuo of MgNPA.

3.3 Frontier molecular orbitals, molecular electrostatic potential maps and contours

Frontier molecular orbitals which are the highest occupied molecular orbital (HOMO) and the lowest unoccupied molecular orbitals (LUMO) play prominent role in chemical process. The selected portion of the energy diagram for molecular orbitals of MgNPA calculated at B3LYP level with basis set 6-31+G(d,p) is presented in Fig. 4. In this diagram, degeneracy tolerance is determined as 0.002 a.u.

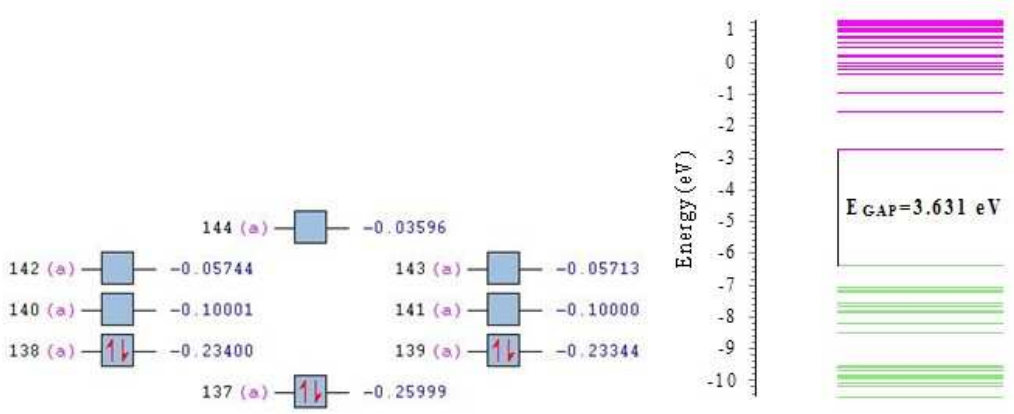

Fig. 4. A certain section of energy diagram of studied complex at B3LYP/6-31+G(d,p) level in gas phase.

The difference of energy between HOMO-1 and HOMO orbital was found very small which determines the fact that both HOMO and HOMO-1 are important to determine chemical reactivity of the complex. As for the unoccupied molecular orbitals, energy of LUMO+1 is close to energy of LUMO. Thus, the activity of LUMO+1 is similar to that of LUMO. According to these results, contour diagrams of related molecular orbitals are calculated and represented in Fig. 5.

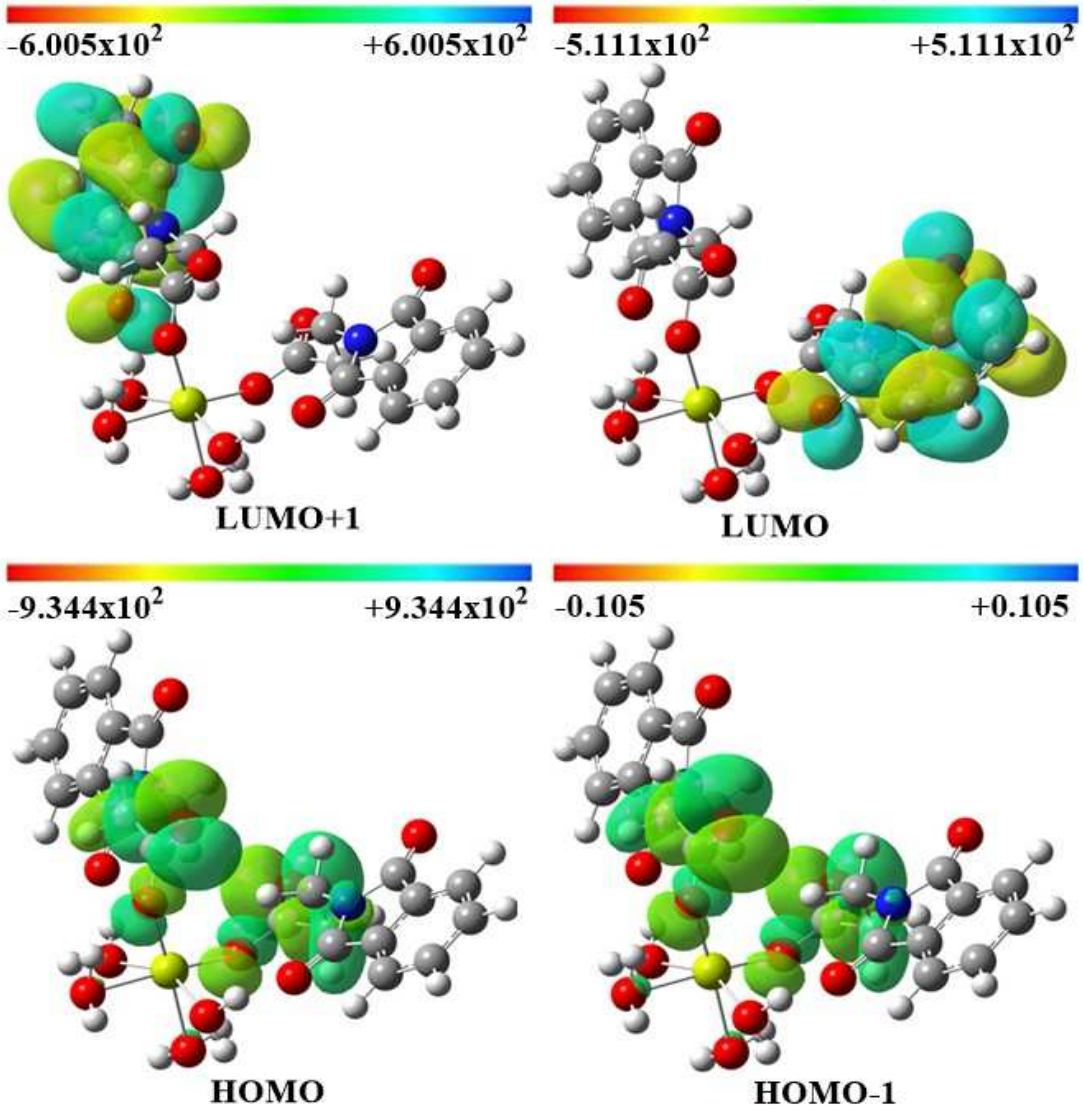

Fig. 5. Contour diagrams for HOMO, HOMO-1, HOMO, LUMO and LUMO+1 molecular orbitals at B3LYP/6-31+G(d,p) level in gas phase for the title complex.

The electron density for molecular orbitals of MgNPA was mapped through color scale which implies electron dense region (between red and green) or electron scarce region (between green and dark blue). There are some balloons in HOMO and LUMO of studied complex. The electrons in HOMO are delocalized in these balloons. If studied complex give electrons, these regions are active in chemical process. As for the LUMO, there is no electrons in this molecular orbital. If mentioned complex accept electrons from appropriate chemical species, these regions are active in this interaction. Therefore, these regions are active in chemical process.

Molecular electrostatic potential (MEP) maps are related to electron density on molecule surface. This map can be used to predict the active sites of complex. MEP map and contour of mentioned complex are calculated at B3LYP/6-31+G(d,p) level and represented in Fig. 6.

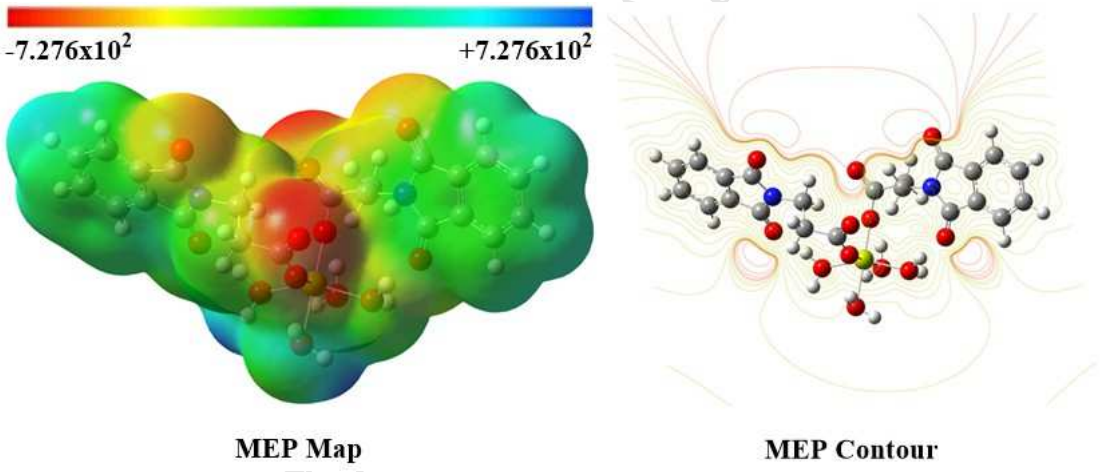

Fig. 6. MEP maps and contours of MgNPA at B3LYP/6-31+G(d,p) level in gas phase

According to color scale, red implies the electron rich region and blue is electronically poor region. These results are related with electrophilic and nucleophilic reactivities. So, colors between red and green in MEP maps are related to electrophilic reactivity. Additionally, the colors between green and blue in MEP maps are related to nucleophilic reactivity. There are red regions around the oxygen atoms on MEP map and it means that environment of oxygen atoms are electrophilic active regions. In MEP contour, there are yellow and red lines. Red lines imply

the electron dense regions. According to these data, electron dense region is environment of oxygen atoms.

3.4 TG-DTA

The TG and DTA curves of NPA and MgNPA are shown in Fig. 7 and the thermo analytical data were summarized in Table 3. The DTA curve of NPA shows two endothermic peaks. The first peak at ~157^{0}C associated with zero mass loss is due to the melting of NPA. The melting point of NPA is 149-151^{0}C [45]. The second endothermic peak at ~328^{0}C is due to the boiling of NPA. This is also supported by 100 % weight loss in 207-352^{0}C temperature range. Finally, the decomposition of NPA vapors start at ~360^{0}C. The shoulders in DTA curve after this temperature are due to the release of different moieties from NPA at different temperatures. The TGA of MgNPA showed that the decomposition was taken in five stages. The first stage occurred with endothermic peak at a maximum temperature of 103ºC. This stage is due to the loss of four water molecules with a weight loss of 7.31 % while the theoretical weight loss 7.41 %. The rest four stages in the range of 111-770ºC showing the decomposition of four N-phthaloyl-ß-alanine. In DTA of MgNPA, the exothermic peak at ~218^{0}C is shown. The removal of four water molecules in first stage leaves the dangling bonds of Mg. The peak at 218^{0}C may be due to bonding of uncoordinated ligand molecules with Mg. The final exothermic peak at 541^{0}C is associated with decomposition of the complex along with the oxidation of Mg. The decomposition is an endothermic process while oxidation of magnesium is an exothermic process. The four stages were associated with a weight loss of 84.77 % and the calculated weight loss value in these four stages was 88.36 %. The found total weight loss value was 93.22 % with a residue equal to 6.78 % which is corresponding to magnesium oxide MgO. These results are in a good agreement with the theoretical values, total loss equal 95.77 % and residual 4.12 %.

Table 3. Thermal Data of Compounds NPA and MgNPA

Compounds/ Codes	Number of Stages	Temp. range (°C)	T_{max} (°C)	Thermogravimetry(TG)			Decomposition Species
				Mass Loss (%) Observed		Mass Loss (%) calculated	
NPA	2	130-206 207-352	157 (+) 328 (+)	0.985 98.405	99.39	100	NPA
MgNPA	5	70-110	103(+)	7.306		7.41	$4H_2O$
		111-200 201-290 291-425 426-770	134(+) 218(-) 332(+) 541(-)	15.947 0.598 26.266 41.957	84.77	88.36	4NPA

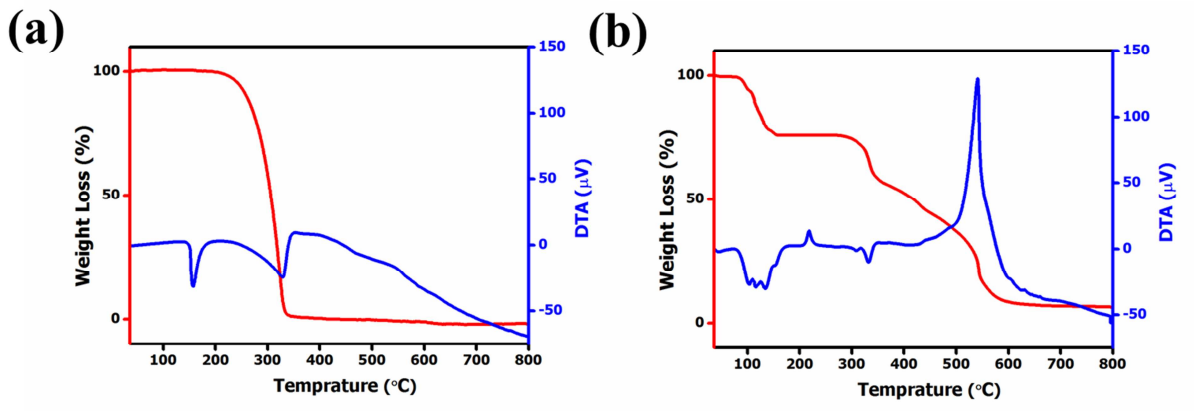

Fig. 7. TG-DTA curves of compounds (a) for NPA and (b) for MgNPA.

3.5 THz spectroscopy measurements

The refractive index and absorption coefficient of MgNPA and NPA are depicted in the Fig. 8. The absorption spectra of NPA shows peaks at 1.84 THz (61.5 cm^{-1}), 2.32 THz (77.6 cm^{-1}), 2.88 THz (96 cm^{-1}) and a shoulder at 1.29 THz (43 cm^{-1}). Wei Ning et. al. [46] has observed a shoulder at 1.23 THz and 1.99 THz for phenylalanine which were absent in the spectra of alanine. This suggests that the shoulder at 1.29 THz and peak at 1.84 THz is due to association of aromatic groups with alanine. Two peaks at 2.23 THz (74 cm^{-1}) and 2.56 THz (85 cm^{-1}) are reported by some authors [46, 47] for L- alanine while these peaks are absent in NPA. We have observed two new peaks at 2.32 THz and 2.88 THz for NPA. The absorption spectra of MgNPA complex shows peaks at 1.26 THz (42 cm^{-1}), 1.82 THz (60.7 cm^{-1}) and 2.82 THz (94 cm^{-1}) which

are slightly shifted to lower frequency than that of NPA. Two new peaks at 1.02 THz (34 cm^{-1}) and 1.52 THz (50.7 cm^{-1}) are also observed in MgNPA which are not present in NPA. These peaks may arise due to different bonding motility in MgNPA.

The refractive index in terahertz frequency range of NPA increased from 1.96 at 0.2 THz to 2.21 at 1.88 THz and then decreases to 2.08 at 3.2 THz. The changes in refractive index corresponding to the absorption peaks can also be observed. The refractive index of MgNPA changes from 1.91 at 0.2 THz to 1.94 at 3.2 THz. The refractive index is higher for the frequencies corresponding to the absorption peaks of MgNPA. The higher refractive index for ligand (NPA) than the complex (MgNPA) is also observed by Turan et. al. [48] for optical frequencies. According to Lorentz-Lorenz equation [49] (B), the higher polarizability of material results in higher refractive index. This suggests that the polarizability of MgNPA is lower than that of NPA. This may be due to stronger bonding in MgNPA that of NPA as was also indicated by different authors. [50, 51]

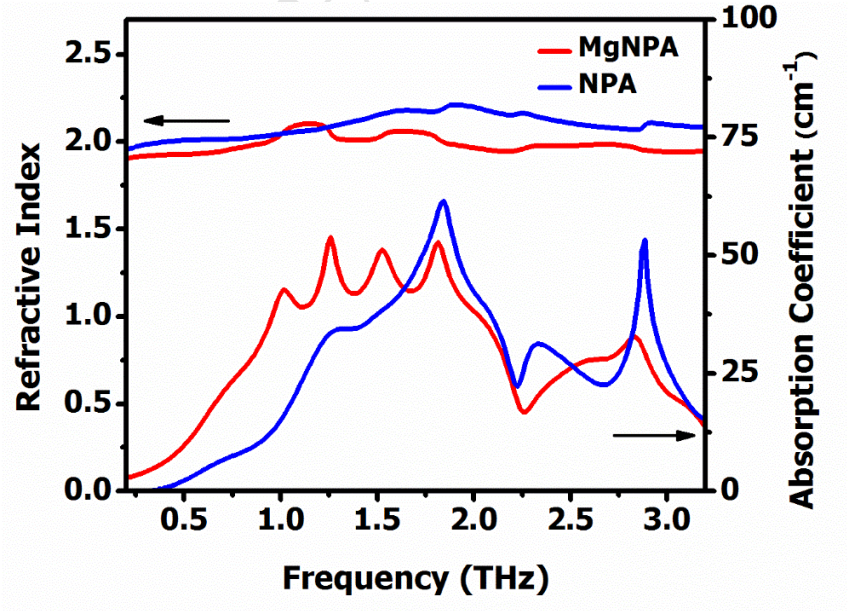

Fig. 8. Refractive index and absorption coefficient of MgNPA and NPA measured using THz-TDS.

3.6 Absorption and Emission Spectroscopy

The transition metal coordination compounds are often used as photoluminescent materials. [52] Alexey et al reported the good luminescent behavior magnesium coordination complexes. [53] The UV-Vis spectrum of NPA and MgNPA recorded in water solution showed two absorption bands in the UV region (Fig. 9a). The bands at λ max range 220-250 nm and 260-300 nm were assigned to ligand-centered (π-π*) and (n-π*) transitions respectively[54, 55]. The optical bandgap (E_g) estimated from the Tauc plot is 4.85eV, the corresponding wavelength λ= 256 nm was used as excitation wavelength to take the fluorescence emission spectra of both ligand and complex MgNPA in solid state, resulted emission at 404 nm and 473 nm. The Tauc' plot and emission spectra are depicted in Fig. 9b and Fig. S1. The ligand emission peaks may be assigned to the $\pi^* \rightarrow \pi$ and $\pi^* \rightarrow$ n transitions. The emission peak positions of ligand and complex are the same. The intensities of emission for both NPA and MgNPA compounds were different. It was observed that no emission originates from the metal-centered MLCT/LMCT excited states because no red or blue shift was observed. Thus the emission bands of both ligand and complex can be attributed to the intra-ligand fluorescent emission. The strong enhancement of the luminescence intensity for MgNPA as compared to the free ligand is perhaps the result of metal–ligand coordination, which effectively increases the rigidity of the ligand and the reduction of energy loss by nonradiative decay. [56-59]

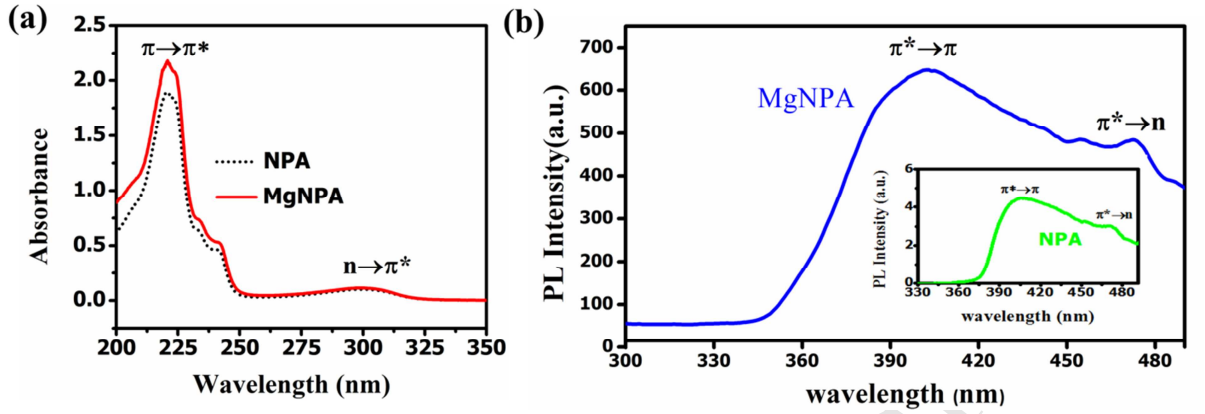

Fig. 9. (a) UV spectra of compounds MgNPA and NPA at concentration of 1×10^{-6} mol dm^{-3} in water solution at 25.0 ± 0.1 ºC, (b) Photoluminescence spectra in solid state for title complex at 25.0 ± 0.1 ºC.

4 Conclusions

The magnesium complex of N-phthaloyl-β-alanine (MgNPA) was synthesized and its crystal structure analyzed by both experimental and computational method. In MgNPA the coordination number of magnesium atom is six with octahedral geometry. The two NPA molecules of ligand coordinated with magnesium atom in a monodentate manner ($\eta^1\mu^1$). The calculated and experimental results of FT-IR for MgNPA had shown good agreement. MEP maps showed electrophilic active zone is mainly due to the oxygen atoms. The result of TG-DTA exhibited that the decomposition of complex is an endothermic process while oxidation of magnesium is an exothermic process. The THz-TDS shows that the characteristic absorption peaks at different frequencies for both ligand and complex. The complexation of NPA with MgNPA results the disappearance of peak at 2.32 THz and emergence of two new peaks at 1.02 THz and 1.52 THz. Further, the refractive index in THz frequency range is also lower for complex than that of ligand. In the fluorescence emission spectra the strong enhancement of the luminescence intensity for MgNPA as compared to the free ligand is the result of metal–ligand coordination.

Acknowledgments

The numerical calculations reported in this paper are performed at TUBITAK ULAKBIM, High Performance and Grid Computing Center (TRUBA Resources). The authors also thank CHEMCRAFT and GABEDIT for allowing using their free internet version. The authors are thankful to Allama Iqbal Open University and Pakistan Institute of Engineering and Applied Sciences (PIEAS) for experimental work and characterization. The authors are also thankful to Mr. Muhammad Mumtaz (NILOP) for his kind cooperation.

Supplementary data

Crystallographic data (excluding structure factors) for the MgNPA had been deposited in the Cambridge Crystallographic Data Center as supplementary publication, CCDC No. 876494. The data can be obtained free of charge on application to CCDC, 12 Union Road, Cambridge CB2 1EZ, UK (fax: (internet) +44 1223 336 033; e-mail: deposit@ccdc.cam.ac.uk). or www at http://www.ccdc.cam.ac.uk].

References

[1] M. Bagherzadeh, A. Ghanbarpour, H.R. Khavasi, Catal. Commun. 65 (2015) 72-75.

[2] H. Furukawa, K.E. Cordova, M. O'Keeffe, O.M. Yaghi, Science 341(6149) (2013) 1230444.

[3] B.-Q. Ma, H.-L. Sun, S. Gao, G.-X. Xu, Inorg. Chem. 40(24) (2001) 6247-6253.

[4] P.D. Beer, P.A. Gale, Angew. Chem. Int. Ed. 40(3) (2001) 486-516.

[5] Y. Zhao, A.-M. Ren, L.-Y. Zou, J.-F. Guo, J.-K. Feng, Theor. Chem. Acc. 130(1) (2011) 61-68.

[6] R.P. Davies, R.J. Less, P.D. Lickiss, A.J. White, Dalton Trans. (24) (2007) 2528-2535.

[7] M. Dinca, J.R. Long, J. Am. Chem. Soc. 127(26) (2005) 9376-9377.

[8] I. Senkovska, S. Kaskel, Eur. J. Inorg. Chem. 2006(22) (2006) 4564-4569.

[9] J.A. Rood, B.C. Noll, K.W. Henderson, Inorg. Chem. 45(14) (2006) 5521-5528.

[10] W. Derave, M.S. Özdemir, R.C. Harris, A. Pottier, H. Reyngoudt, K. Koppo, J.A. Wise, E. Achten, J. Appl. Physiol. 103(5) (2007) 1736-1743.

[11] M.E. Vázquez, J.B. Blanco, B. Imperiali, J. Am. Chem. Soc. 127(4) (2005) 1300-1306.

[12] Ö. Tamer, M.H. Bhatti, U. Yunus, D. Avcı, Y. Atalay, M. Nadeem, S.R. Shah, M. Helliwell, J. Mol. Struct. 1125 (2016) 315-322.

[13] A. Podborska, M. Wojnicki, J. Mol. Struct. 1128 (2017) 117-122.

[14] K. Lyczko, J. Mol. Struct. 1127 (2017) 549-556.

[15] E. Aktan, A.B. Gündüzalp, Ü.Ö. Özmen, J. Mol. Struct. 1128 (2017) 775-784.

[16] H. Keypour, M. Shayesteh, M. Rezaeivala, K. Sayin, J. Mol. Struct. 1112 (2016) 110-118.

[17] K. Sayin, N. Kurtoglu, M. Kose, D. Karakas, M. Kurtoglu, J. Mol. Struct. 1119 (2016) 413-422.

[18] C.D. Stoik, M.J. Bohn, J.L. Blackshire, Opt. Express 16(21) (2008) 17039-17051.

[19] K. Kawase, Y. Ogawa, Y. Watanabe, H. Inoue, Opt. Express 11(20) (2003) 2549-2554.

[20] S. Mehboob, M. Mehmood, M. Ahmed, J. Ahmad, M.T. Tanvir, I. Ahmad, S.M.u. Hassan, Mater. Chem. Phys. 191 (2017) 62-69.

[21] S. Mehboob, M. Mehmood, M. Ahmed, J. Ahmad, M.T. Tanvir, I. Ahmad, Infrared Phys. Technol. 78 (2016) 200-208.

[22] A. Mazady, A. Rivera, M. Anwar, Solid.State Electron. 101 (2014) 8-12.

[23] P. Bawuah, P. Silfsten, A. Sarkar, K. Kordas, J.-P. Mikkola, K.-E. Peiponen, Vib. Spectrosc 68 (2013) 241-245.

[24] J. Han, B.K. Woo, W. Chen, M. Sang, X. Lu, W. Zhang, J. Phys. Chem. C 112(45) (2008) 17512-17516.

[25] W. Wei-Ning, L.I. Hong-Qi, Z. Yan, Z. Cun-Lin, Acta Physico-Chimica Sinica 25(10) (2009) 2074-2079.

[26] Y. Ueno, K. Ajito, Anal. Sci. 23(7) (2007) 803-807.

[27] A.G. Markelz, A. Roitberg, E.J. Heilweil, Chem. Phys. Lett. 320(1–2) (2000) 42-48.

[28] Q.-M. Qiu, M. Liu, Z.-F. Li, Q.-H. Jin, X. Huang, Z.-W. Zhang, C.-L. Zhang, Q.-X. Meng, J. Mol. Struct. 1062 (2014) 125-132.

[29] Y. Yuan, H.-L. Han, S. Lin, Y.-Z. Cui, M. Liu, Z.-F. Li, Q.-H. Jin, Y.-P. Yang, Z.-W. Zhang, Polyhedron 119 (2016) 184-193.

[30] Y.-S. Yang, M. Liu, Y.-P. Yang, Q.-H. Jin, Z.-F. Li, X.-N. Xue, Z.-J. Zhang, W.-J. Zheng, Polyhedron 93 (2015) 66-75.

[31] N. Barooah, R.J. Sarma, A.S. Batsanov, J.B. Baruah, Polyhedron 25(1) (2006) 17-24.

[32] R. Dennington, T. Keith, J. Millam, Semichem Inc., Shawnee Mission, KS (2009).

[33] M. Frisch, G. Trucks, H. Schlegel, G. Scuseria, M. Robb, J. Cheeseman, G. Scalmani, V. Barone, B. Mennucci, G. Petersson, Phys. Rev. B: Condens. Matter Mater. Phys 37 (1988) 785.

[34] M. Frisch, G. Trucks, H. Schlegel, G. Scuseria, M. Robb, J. Cheeseman, G. Scalmani, V. Barone, B. Mennucci, G. Petersson, Gaussian 09 Revision A. 02. Wallingford: Gaussian, Inc, 2009.

[35] M. Frisch, G. Trucks, H. Schlegel, G. Scuseria, M. Robb, J. Cheeseman, G. Scalmani, V. Barone, B. Mennucci, G. Petersson, Inc., Wallingford, CT (2009).

[36] M. Frisch, G. Trucks, H. Schlegel, G. Scuseria, M. Robb, J. Cheeseman, G. Scalmani, V. Barone, B. Mennucci, G. Petersson, Inc.: Wallingford, CT (2009).

[37] M. Frisch, G. Trucks, H. Schlegel, G. Scuseria, M. Robb, J. Cheeseman, G. Scalmani, V. Barone, B. Mennucci, G. Petersson, Inc., Wallingford, CT (2009).

[38] J.K. Kibet, Kabarak j. res. innov. 4(1) (2016) 49-61.

[39] A.R. Allouche, J. Comput. Chem. 32(1) (2011) 174-182.

[40] A.D. Becke, J. Chem. Phys. 98(7) (1993) 5648-5652.

[41] C. Lee, W. Yang, R.G. Parr, Phys. Rev. B 37(2) (1988) 785.

[42] G.M. Sheldrick, Acta Crystallogr. Sect. A: Found. Crystallogr. 64(1) (2007) 112-122.

[43] K. Nakamoto, Infrared and Raman spectra of inorganic and coordination compounds, Wiley Online Library1986.

[44] G. Kumar, M. Srivastava, Rev Chim Miner 16 (1979) 14-8.

[45] S. Zav'yalov, O. Dorofeeva, E. Rumyantseva, L. Kulikova, G. Ezhova, N. Kravchenko, A. Zavozin, Pharm. Chem. J. 36(8) (2002) 440-442.

[46] W.-N. Wang, H.-Q. Li, Y. Zhang, C.-L. Zhang, Acta Physico-Chimica Sinica 25(10) (2009) 2074-2079.

[47] M. Yamaguchi, F. Miyamaru, K. Yamamoto, M. Tani, M. Hangyo, Appl. Phys. Lett. 86(5) (2005) 053903.

[48] N. Turan, B. Gündüz, H. Körkoca, R. Adigüzel, N. Çolak, K. Buldurun, J. Mex. Chem. Soc. 58(1) (2014) 65-75.

[49] S. Musikant, Optical Engineering, New York: Dekker, 1985 (1985).

[50] S. Mehboob, M. Mehmood, M. Ahmed, J. Ahmad, M.T. Tanvir, I. Ahmad, S.M. ul Hassan, Mater. Chem. Phys. 191 (2017) 62-69.

[51] M. Barsoum, M. Barsoum, Fundamentals of ceramics, CRC press2002.

[52] P.D. Fleischauer, P. Fleischauer, Chem. Rev. 70(2) (1970) 199-230.

[53] A. Gusev, E. Braga, V. Shul'gin, K. Lyssenko, I. Eremenko, L. Samsonova, K. Degtyarenko, T. Kopylova, W. Linert, Materials 10(8) (2017) 897.

[54] H. Hadadzadeh, M.M. Olmstead, A.R. Rezvani, N. Safari, H. Saravani, Inorg. Chim. Acta 359(7) (2006) 2154-2158.

[55] G. Mansouri, A.R. Rezvani, H. Hadadzadeh, H.R. Khavasi, H. Saravani, J. Organomet. Chem. 692(17) (2007) 3810-3815.

[56] J. Zhang, Y.R. Xie, Q. Ye, R.G. Xiong, Z. Xue, X.Z. You, Eur. J. Inorg. Chem. 2003(14) (2003) 2572-2577.

[57] R. Wang, L. Han, F. Jiang, Y. Zhou, D. Yuan, M. Hong, Cryst. Growth Des. 5(1) (2005) 129-135.

[58] L.-L. Wen, D.-B. Dang, C.-Y. Duan, Y.-Z. Li, Z.-F. Tian, Q.-J. Meng, Inorg. Chem. 44(20) (2005) 7161-7170.

[59] Y. Jia, H. Li, Q. Guo, B. Zhao, Y. Zhao, H. Hou, Y. Fan, Eur. J. Inorg. Chem. 2012(18) (2012) 3047-3053.

Crystal structure, thermal, luminescent and terahertz time domain spectroscopy of magnesium N-phthaloyl-β-alaninate: A combined experimental and theoretical study

Research Highlights

- Synthesis and growth of single crystals for MgNPA.
- Optimization of complex carried by B3LYP with basis set, 6-31+G(d,p).
- TD-THz spectroscopy characterized well MgNPA and NPA.
- Decrease in refractive index for NPA due to complexation of NPA with Mg.